

LETTER | MAY 13 2022

Broadband polarization insensitivity and high detection efficiency in high-fill-factor superconducting microwire single-photon detectors

Dileep V. Reddy ; Negar Otoooshi; Sae Woo Nam; Richard P. Mirin ; Varun B. Verma



APL Photonics 7, 051302 (2022)

<https://doi.org/10.1063/5.0088007>



Articles You May Be Interested In

Large active-area superconducting microwire detector array with single-photon sensitivity in the near-infrared

Appl. Phys. Lett. (June 2023)

High-resistivity niobium nitride films for saturated-efficiency SMSPDs at telecom wavelengths and beyond

Appl. Phys. Lett. (April 2023)

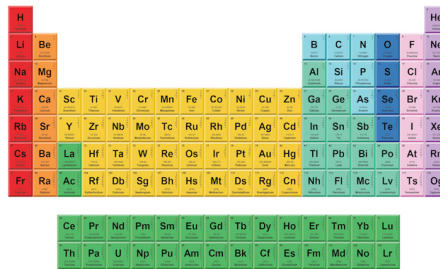
Large single-photon detector opens door to high energy physics, dark matter, and more

Scilight (June 2023)



THE MATERIALS SCIENCE MANUFACTURER®

Now Invent.TM



American Elements
Opens a World of Possibilities

...Now Invent!

Broadband polarization insensitivity and high detection efficiency in high-fill-factor superconducting microwire single-photon detectors

Cite as: APL Photon. 7, 051302 (2022); doi: 10.1063/5.0088007

Submitted: 11 February 2022 • Accepted: 26 April 2022 •

Published Online: 13 May 2022



View Online



Export Citation



CrossMark

Dileep V. Reddy,^{1,2,a)} Negar Otrrooshi,^{1,2} Sae Woo Nam,² Richard P. Mirin,² and Varun B. Verma²

AFFILIATIONS

¹ Department of Physics, University of Colorado, Boulder, Colorado 80309, USA

² National Institute of Standards and Technology, Boulder, Colorado 80305, USA

^{a)} Author to whom correspondence should be addressed: dileep.reddy@nist.gov

ABSTRACT

Single-photon detection via absorption in current-biased nanoscale superconducting structures has become a preferred technology in quantum optics and related fields. Single-mode fiber packaged devices have seen new records set in detection efficiency, timing jitter, recovery times, and the largest sustainable count rates. The popular approaches to decreasing polarization sensitivity have resorted to the deposition of a high-index dielectric layer in between the nanowires or the introduction of geometrically symmetric nanowire meanders, such as spirals and fractals, in the active area. The former method yields limited success, while constraints on bending radii, and by extension fill factors in the latter limits their maximum efficiency. The discovery of single-photon sensitivity in micrometer-scale superconducting wires enables novel meander patterns with no effective upper limit on the fill factor. This work demonstrates simultaneous low-polarization sensitivity (1.02 ± 0.008) and high detection efficiency (>91.8% to better than one standard deviation at 2×10^5 counts/s) across a 40 nm bandwidth centered at 1550 nm in 0.51 μm wide microwire devices made of silicon-rich tungsten silicide, sporting a new candelabra-style meander pattern with a fill factor of 0.91 in the active area. These devices boasted efficiencies of 96.5%–96.9% \pm 0.5% at 1×10^5 counts/s for 1550 nm light.

© 2022 Author(s). All article content, except where otherwise noted, is licensed under a Creative Commons Attribution (CC BY) license (<http://creativecommons.org/licenses/by/4.0/>). <https://doi.org/10.1063/5.0088007>

I. INTRODUCTION

Superconducting nanowire single-photon detectors (SNSPDs) are a premier technology for applications that require fast, high-efficient detection and high-timing resolution. Their utility spans diverse areas, such as fundamental research,¹ communications,^{2,3} metrology,⁴ remote sensing,⁵ materials research,⁶ and astronomy.^{7,8} Such detectors in a single-mode fiber-packaged form have been fruitfully employed in several ground-breaking quantum-optics experiments.^{9–16} Within the past five years, fiber-packaged SNSPDs have seen new records set in diverse figures-of-merit, such as system-detection efficiency (SDE),^{17–19} timing jitter,²⁰ and low dark counts.²¹ The field is making advances toward joint high performance in multiple metrics simultaneously. One such goal is high SDE coupled with low polarization sensitivity.

We define polarization sensitivity (PS) for a device as the ratio of the maximum to minimum SDE across all input polarization states of photons. Traditional fiber-coupled SNSPDs have consisted of nanowire meanders covering the active area (where photons are expected to be absorbed) in a zigzag pattern. The geometry forms a grating-like structure of parallel strips of superconductor spaced by a dielectric. Consequently, SNSPDs have inherently possessed a non-unity PS.^{22–25} While such meanders allow for unity PS at a specific wavelength via cleverly engineered anti-reflection coatings,²⁶ reliable unity-PS across significant bandwidths has remained unrealized in high-efficiency devices. Applications that require high efficiency and throughput^{11,27,28} often use polarization controllers before directing light to the detectors, which is an extra burden to the system and may cause some optical loss. High-SDE devices with either unity or infinite PS (meaning no sensitivity to

one polarization) would obviate the need for such measures. Such detectors would also close a security loophole in standard phase-encoding quantum-key distribution implementations.²⁹

Historical approaches to achieving unity PS have sought to spatially symmetrize the nanowire-meander geometries. PS values of 1.02–1.04 have been measured in spiral SNSPDs since 2008^{30–32} with limited SDE. In 2012, Verma *et al.* fabricated a two-layer 3D-SNSPD with perpendicularly oriented meanders and showed a PS of 1.02 with an SDE of 87.7%.³³ Space-filling fractals, such as Sierpinski or Hilbert curves, have also been studied as a means of introducing discrete rotational symmetries into nanowire meanders.³⁴ The fractal approach has seen steady improvement^{35,36} and has recently realized a PS of 1.02 at 91% efficiency.³⁷ The introduction of turns and hairpin bends in the active area renders the outer-radius regions of such fractal-meander nanowires relatively insensitive to photons,^{37,38} thus limiting their efficiency. Other innovations that do not symmetrize the meander geometry have focused on high-refractive index dielectric media surrounding the nanowires to reduce the effective grating-index contrast.^{23–25,39,40} Alternatively, instead of minimizing PS, the deliberate introduction of grating-like asymmetries in the optical stack using dielectric or metal slots to maximize PS has also been considered.^{41,42}

The year 2020 witnessed several observations of micrometer-wide superconducting structures being sensitive to single photons when current biased. While such scales were trivial for higher-energy photons, such as x-rays,⁴⁴ Korneeva *et al.* showed the first such instance for near-infrared (IR) photons.⁴⁵ Specifically, they observed that 3.3 nm thick, 2 μm wide molybdenum silicide (MoSi) microstrips could detect photons of wavelength 1 μm . Chiles *et al.* modified their tungsten silicide (WSi) recipe to increase the stoichiometric proportion of silicon and demonstrated near-IR photon sensitivity in wires as wide as 4 μm .⁴⁶ Similar results have been observed in niobium nitride (NbN).⁴⁷ This new result has spurred interest in gaining a better understanding of the photon-detection mechanism in such devices. It has also enabled a new class of superconducting microwire single-photon detectors (SMSPDs), resulting in new active-area records being set in free-space coupled devices.^{48–51}

Superconducting microwires have already been used to make spiral-meander SMSPDs by Xu *et al.*,⁵² achieving a PS of 1.03 with 92.2% efficiency at the wavelength 1550 nm. The maximum fill factor they reported was 0.8. The presence of curvature in the

current's path in the active area is still suboptimal for SDE due to current crowding.^{38,53} The traditional meander design (parallel strips of superconductor separated by dielectric medium) when conjoined with micrometer-scale wire widths offers a trivial means of reaching near-unity fill factors. This would reduce the relative preponderance of edges in the active area, which differentially absorb TE (transverse-electric) and TM (transverse-magnetic) polarizations.^{22–25} The minimum gap between parallel, straight segments of superconductor in a traditional meander is limited by the resolution of the electron-beam writing and etch process and is typically on the order of 40–100 nm. At such gap widths, the current crowding at the inner radii of the hairpin bends^{38,54,55} of a traditional meander would be exacerbated for microwires, causing such a device to latch at a very low bias current.⁵³ The current-crowding effect is nullified if the fill factor at a hairpin bend is at or below 0.33.^{38,56}

In this work, we introduce the candelabra meander (see the [supplementary material](#)), which utilizes optimized 90° and 180° bending primitives (defined in the python CAD-layout library phidl⁴³) to slowly turn the microwire outside of the active area, enabling us to maintain a high active-area fill factor while minimizing current crowding [see Fig. 1(a)]. The design is inspired by similar structures used in optical waveguides, where a specific length is to be maintained within an area/footprint constraint while minimizing optical loss at the bends. This solution has recently been independently proposed by Jönsson *et al.*⁵⁶ The candelabra meander requires a longer length of microwire to cover the same active area as a traditional meander [see Fig. 1(b)], resulting in increased kinetic inductance. Using the silicon-rich tungsten silicide (WSi) recipe developed by Chiles *et al.*,⁴⁶ we fabricated fiber-coupled, candelabra-meander SMSPDs with 0.51 μm wide wires and a 0.91 fill factor in the active area. These meanders were embedded in the Bragg-grating and three-layer anti-reflection-coating based optical stack that was previously employed to break the SDE record.¹⁷ We show that these devices have a near-unity PS of better than 1.02 and a high SDE of better than 91.8% (by better than one standard deviation at 2×10^5 counts/s) over a wide bandwidth of 40 nm centered at a wavelength of 1550 nm and SDEs in the range of 96.5%–96.9% \pm 0.5% (at 1×10^5 counts/s) at 1550 nm. This paves the way for the utilization of superconducting microwires for lowering polarization sensitivity in highly efficient single-photon detectors.

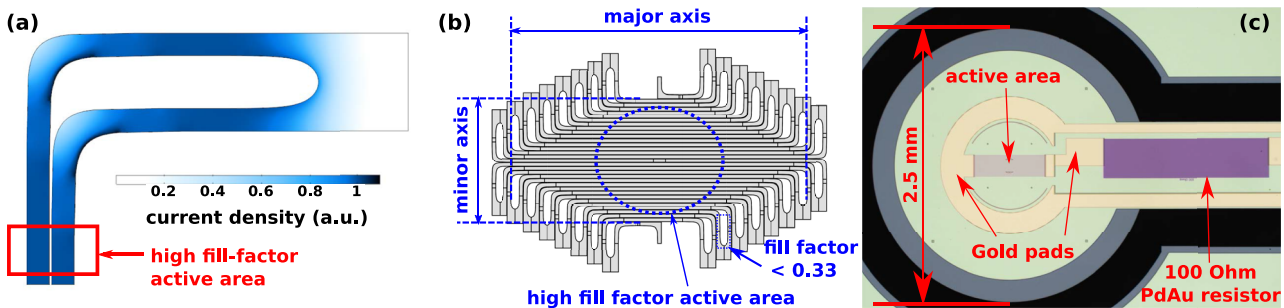


FIG. 1. (a) Simulated current density in a candelabra-style hair-pin bend⁴³ (see the [supplementary material](#)). (b) Schematic of candelabra meander nanowire showcasing high fill factor. (c) Optical micrograph of a device chip showing a speed-up PdAu resistor.

II. FABRICATION AND EXPERIMENTAL SETUP

The SMSPDs presented here were fabricated on a 76.2 mm diameter silicon wafer. Thirteen alternating layers of silicon dioxide (SiO_2 , thickness 266.75 ± 0.84 nm) and amorphous silicon (αSi , thickness 141.7 ± 0.27 nm)—starting with SiO_2 —were deposited onto the substrate using plasma-enhanced chemical vapor deposition (PECVD), forming a 6.5-period Bragg reflector at 1550 nm. We then deposited gold terminals and $100\ \Omega$ palladium-gold (PdAu) speed-up resistors¹⁷ [see Fig. 1(c)] using a photolithographic lift-off process. We then deposited a 2.2 nm layer of silicon-rich WSi⁴⁶ with a 2 nm thick αSi capping layer using a magnetron sputtering tool. A candelabra meander for $0.51\ \mu\text{m}$ wide wires and 50 nm gap width was then patterned onto an electron-beam resist layer.

Due to the ultra-thin nature of the WSi layer (which limits the amount of light absorption per transmissive pass), we needed to cover a larger active area than in comparable optical stacks that utilize other materials and thicknesses¹⁷ to account for the extra beam divergence. Therefore, the candelabra meander covered a rhomboidal active area with a minor axis of length $80\ \mu\text{m}$ and a major axis of length $174\ \mu\text{m}$ [the shortest possible major axis for a given minor axis length, fill factor, and bend radius, see Fig. 1(b)]. The meander pattern was then transferred onto the WSi layer using SF_6 -based reactive-ion etching. We then deposited a three-layer coating of αSi (28 ± 0.27 nm), SiO_2 (123.1 ± 0.84 nm), and αSi (183.5 ± 0.27 nm) in that order onto the microwire layer. These thicknesses were determined to minimize the reflection of vertically incident 1550 nm light using rigorous coupled-wave analysis (RCWA) simulations.^{57,58} Vias were then selectively etched into the top three dielectric layers to enable wire bonding access to the gold pads. Deep-reactive-ion etching was then used to etch through the wafer substrate in a keyhole pattern [see Fig. 1(c)], which enabled easy liberation of the device dies and their mounting into the fiber-ferrule self-aligning package developed by Miller *et al.*⁵⁹ SMF28e+ fiber pigtails terminating at AR-coated, 2.5 mm-diameter ceramic ferrules were then inserted into the self-aligning packages.

Four devices from a single wafer were mounted inside a sorption-based cryostat and cooled to 720–730 mK. The devices were electrically accessible through SMA ports and optically accessible through splicing into the bare ends of the fiber pigtails outside of the cryostat. The system-detection efficiency (SDE) reported here is defined as the probability for the device to register a detection given that a photon is launched into the fiber pigtail.¹⁷ All measurements were performed using a highly attenuated, tunable, continuous-wave laser passed through a 1×2 optical switch and two different types of polarization controllers. An all-fiber polarization controller was used for algorithmic polarization optimizations at various wavelengths. A free-space polarization controller was later used to fully scan the Bloch sphere at 1550 nm. A NIST-calibrated power meter, and a rack-mounted, “monitoring” power meter were used for all equipment calibrations.¹⁷ The devices were quasi-current-biased using a bias tee, a $100\ \text{k}\Omega$ series resistor, and a programmable voltage source. The detection pulses were amplified using two room-temperature RF amplifiers, conditioned into square pulses using comparators, and plugged into an electronic pulse counter. The design, fabrication, calibration procedures, and

error analysis are described in greater detail in the [supplementary material](#).

III. MEASUREMENT RESULTS AND DISCUSSION

One out of the four mounted devices was found to be electrically open when cooled down. We therefore only present the results for the remaining three devices, labeled D1, D2, and D3. The kinetic inductance of 2.2 nm thick, Si-rich WSi was measured to be $275\ \text{pH}/\text{sq}$, which is nearly thrice the typical value for SNSPDs. This, along with the bigger active area required, counteracts the gains made in decreasing total inductance through micrometer-scale wire widths. We fabricated a $100\ \Omega$ speed-up resistor in series with the microwire to gain a factor of two in recovery time,¹⁷ yielding a value of $\approx 120\ \text{ns}$. The width of the comparator-conditioned square pulses averaged around 175 ns [see Fig. 2(a)]. The square pulses showed a high variance in temporal width due to electronic noise affecting the hysteresis–voltage threshold trigger set at the comparators. Figure 2(b) shows the counts vs current bias for detector D1 at 2.3×10^5 counts/s and 1550 nm photon wavelength. All three

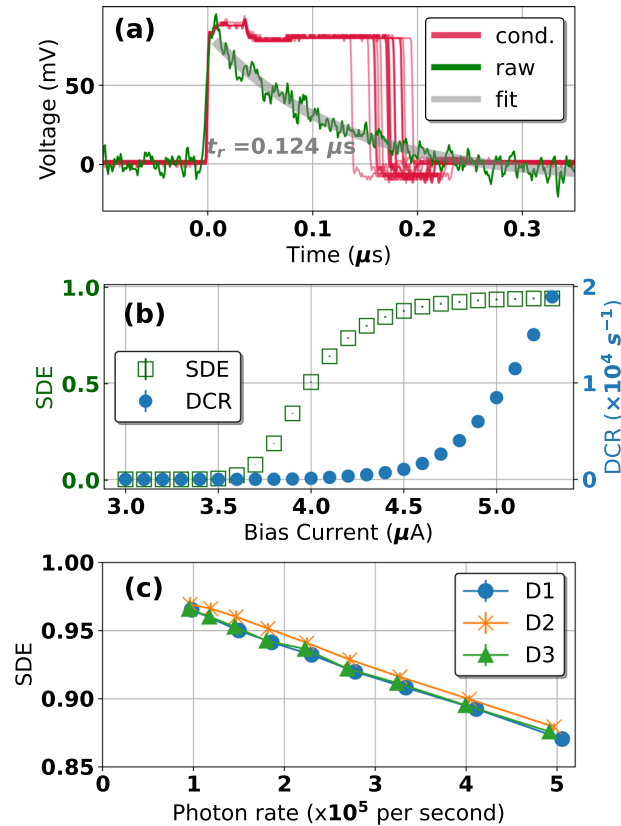


FIG. 2. (a) The raw amplified RF-pulse from device D1 as well as twenty comparator-conditioned pulses vertically scaled-down by a factor of 10. (b) The dark-count rate (DCR) and the system-detection efficiency (SDE) vs bias-current curve at 1550 nm for device D1 at about 2.3×10^5 detections/s in the saturated region. (c) The SDE for various incident photon rates for all three devices biased at $5\ \mu\text{A}$ for 1550 nm photons.

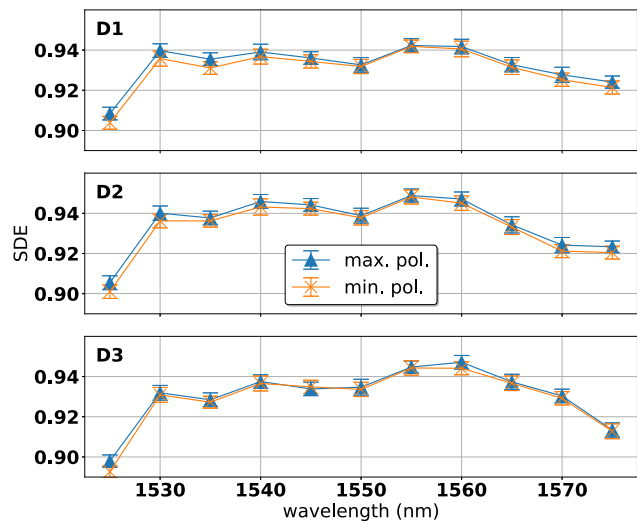


FIG. 3. SDE vs wavelength for all three detectors (D1, D2, D3) at count-rates of $2 \times 10^5/\text{s}$. The rates were maximized and minimized (see the legend) at a constant incident photon rate using an all-fiber polarization controller and the python nlopt library.

detectors showed internal saturation at such count rates, with a dark-count rate of $10^4/\text{s}$ when biased at $5\ \mu\text{A}$.

Figure 2(c) shows the measured SDE at optimal polarization (optimized using the all-fiber polarization controller and the python nlopt library) vs the $1550\ \text{nm}$ photon rate for all three devices. The pile-up effect resulting from the $\approx 175\ \text{ns}$ conditioned-square-pulse reset time,^{50,61} along with any residual device nonlinearity, results in a detection-rate dependent SDE. The standard error bars on the SDE estimate are $\pm(0.39\text{--}0.42)\%$ at a photon rate of $2.3 \times 10^5/\text{s}$, and $\pm(0.49\text{--}0.52)\%$ at photon rates of $1 \times 10^5/\text{s}$ (see the supplementary material). The SDE at photon rates of $10^5/\text{s}$ is around 96.5%–96.9% across the three devices, which is comparable to high-efficiency SNSPDs with 100 ns recovery times.¹⁷ The SDE vs photon rate trend line indicates that these devices are asymptotically fully efficient at ultra-low photon rates and that no light is being lost due to beam

divergence. We designate a rate of $2 \times 10^5/\text{s}$ as a conservative, dominant regime of application and report efficiencies and polarization sensitivities at these light levels in the abstract and conclusion of this Letter. Furthermore, we report all efficiencies at a bias current of $5\ \mu\text{A}$, which is about 94%–96% of the switching current across all three devices.

In Fig. 3, we plot the SDE for all three devices measured at a photon rate of $2 \times 10^5/\text{s}$ across the wavelength range of $1525\text{--}1575\ \text{nm}$. The nlopt python library was used to find the settings for the all-fiber polarization controller that maximized and minimized the SDE at a given incident light level. All three detectors showed mean SDEs greater than 92% in the $1530\text{--}1570\ \text{nm}$ wavelength range. For reference, the maximum possible SDE (limited due to pile-up effect^{62,63}) for devices with a dead-time of 175 ns at a continuous input photon rate of $2 \times 10^5/\text{s}$ is 96.5%. This procedure indicated that the all-fiber-controller-derived PS did not exceed 1.006 across the entire bandwidth measured. The PS, in some instances, was measured to be very close to unity, resulting in some difficulty in optimization for the nlopt library. The optimization step for device D3 at $1545\ \text{nm}$ took nearly half an hour to halt for both maximization and minimization, resulting in a “min. pol.” mean-SDE value exceeding the “max. pol.” mean-SDE value.

The all-fiber polarization controller is not guaranteed to sample the entire space of polarization states. Therefore, we replaced it with a free-space polarization controller, which transmits the light in free-space through a linear polarizer, a quarter-wave plate, and a half-wave plate, all three of which are mounted on controllable rotary mounts in that order. This controller was used to scan the entire Bloch-sphere of polarization states. Figure 4 shows plots for transmission-corrected (see the supplementary material) counts normalized to the maximum counts across 21×21 equally spaced polarization settings on the Bloch sphere for all three detectors. The counts were measured at an average count rate of $2.3 \times 10^5/\text{s}$ while the detectors were biased at $5\ \mu\text{A}$, and the measurement took 20 min for each device. Both dark counts and laser power had to be monitored at each polarization setting. A further 20 min was required after each measurement session (per device) to measure the free-space polarization controller transmission correction using two power meters at classical light levels (see the supplementary material). This measurement yielded PS of $1.018\text{--}1.021 \pm 0.008$ for

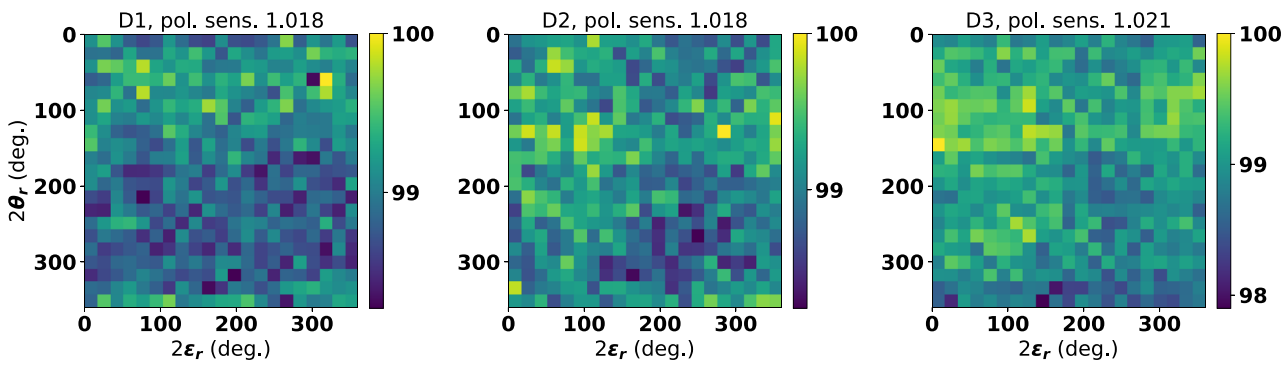


FIG. 4. Normalized count rates at a constant photon rate (of about $2.3 \times 10^5/\text{s}$) with polarization state varied over the entire Bloch sphere using a free-space polarization controller. $2\theta_r$ and $2\epsilon_r$ are the angles of “longitude” and “latitude,” respectively, on the lab-frame Bloch sphere. See subplot titles for detector numbers.

the three devices without any smoothing function applied to the plotted data. We report a conservative value of 1.02 ± 0.008 for PS for our devices in the abstract and conclusion of this Letter.

The microwire recipe used in these devices⁴⁶ required the superconducting layer to be ultra-thin at around 2.2 nm. This is thinner than typical for microwire devices explored thus far.^{45,47,48,52} This resulted in a larger active-area requirement, causing a large kinetic inductance. We employed a speed-up resistor to improve the recovery time. This, along with the substantial length of the candelabra meander, resulted in a large timing jitter of 1.5 ns. The jitter in a similar device without the speed-up resistor was measured to be 170 ps, indicating an impedance-mismatch near the resistor causing electronic reflections at higher RF frequencies. The absence of the speed-up resistor doubled the recovery time and was detrimental to device efficiency. The fill factor of 0.91 has not been optimized. We have merely maximized the fill factor for a given e-beam lithography resolution and microwire width that has shown saturation in internal efficiency for 1550 nm light.

The candelabra meander, when used in conjunction with superconducting microwires, can trivially hit near-unity PS values³⁷ due to their large fill-factors in the active area. Additionally, the absence of bends within the active area can ensure that the microwires are photon sensitive across their entire lateral width, enabling simultaneous near-unity-PS and high-SDE single-photon detection across a wide range of wavelengths. This capability will prove fruitful for quantum optics experiments involving wavelength-division multiplexing, or time-frequency entanglement spanning the low-loss C-band from fiber-optical communications.

IV. CONCLUSION

We introduced the candelabra meander as a new geometry for superconducting nanowire and microwire single-photon detectors. This meander enables high-fill factors in the active area without the deleterious effects of current crowding at the hairpin bends that plagued the traditional meander geometry. We utilized this in the fabrication of WSi-based SMSPDs with 0.51 μm wide microwires and a fill factor of 0.91 in the active area. We embedded the SMSPDs in the Bragg-reflector-based optical stack optimized for high efficiency detection of 1550 nm photons. We then fiber-packaged these devices and measured their polarization sensitivities and system-detection efficiencies at various wavelengths and photon rates in the near-IR region. We showed that this design achieves a PS of 1.02 ± 0.008 and high efficiencies of greater than 92% across a 40 nm bandwidth centered at 1550 nm. This furthers the goal of the development of fiber-coupled single-photon detectors with joint high performance for multiple measures.

SUPPLEMENTARY MATERIAL

The [supplementary material](#) contains three sections: Section I provides some details about device design and fabrication. Section II goes through the entire system-detection efficiency measurement setup, details the algorithms for the measurement and data processing scripts, as well as the error analysis. Section III covers the polarization sensitivity measurement using the free-space polarization controller.

ACKNOWLEDGMENTS

The authors would like to acknowledge Igor Veyshenker for providing them with power-meter calibration. They thank Dr. Gautam A. Kavuri for help with timing-jitter measurements. They also thank Professor Juliet Gopinath and her group for accommodating their cryostat and experimental setup in their laboratory space in the EECE department at the University of Colorado, Boulder.

AUTHOR DECLARATIONS

Conflict of Interest

The authors have no conflicts to disclose.

DATA AVAILABILITY

The data that support the findings of this study are openly available in Zenodo at <https://doi.org/10.5281/zenodo.6036210> and available from the corresponding author upon reasonable request.

REFERENCES

- ¹Y. Hochberg, I. Charaev, S.-W. Nam, V. Verma, M. Colangelo, and K. K. Berggren, *Phys. Rev. Lett.* **123**, 151802 (2019).
- ²Y. Mao, B.-X. Wang, C. Zhao, G. Wang, R. Wang, H. Wang, F. Zhou, J. Nie, Q. Chen, Y. Zhao *et al.*, *Opt. Express* **26**, 6010 (2018).
- ³J.-P. Chen, C. Zhang, Y. Liu, C. Jiang, W. Zhang, X.-L. Hu, J.-Y. Guan, Z.-W. Yu, H. Xu, J. Lin *et al.*, *Phys. Rev. Lett.* **124**, 070501 (2020).
- ⁴S. Slussarenko, M. M. Weston, H. M. Chrzanowski, L. K. Shalm, V. B. Verma, S. W. Nam, and G. J. Pryde, *Nat. Photonics* **11**, 700–703 (2017).
- ⁵J. Zhu, Y. Chen, L. Zhang, X. Jia, Z. Feng, G. Wu, X. Yan, J. Zhai, Y. Wu, Q. Chen *et al.*, *Sci. Rep.* **7**, 15113 (2017).
- ⁶L. Chen, D. Schwarzer, J. A. Lau, V. B. Verma, M. J. Stevens, F. Marsili, R. P. Mirin, S. W. Nam, and A. M. Wodtke, *Opt. Express* **26**, 14859 (2018).
- ⁷Q. Zhuang, Z. Zhang, and J. H. Shapiro, *Phys. Rev. A* **97**, 032329 (2018).
- ⁸E. Khabiboulline, J. Borregaard, K. De Greve, and M. Lukin, *Phys. Rev. Lett.* **123**, 070504 (2019).
- ⁹H. Shibata, T. Honjo, and K. Shimizu, *Opt. Lett.* **39**, 5078 (2014).
- ¹⁰P. B. Dixon, D. Rosenberg, V. Stelmakh, M. E. Grein, R. S. Bennink, E. A. Dauler, A. J. Kerman, R. J. Molnar, and F. N. C. Wong, *Phys. Rev. A* **90**, 043804 (2014).
- ¹¹L. K. Shalm, E. Meyer-Scott, B. G. Christensen, P. Bierhorst, M. A. Wayne, M. J. Stevens, T. Gerrits, S. Glancy, D. R. Hamel, M. S. Allman *et al.*, *Phys. Rev. Lett.* **115**, 250402 (2015).
- ¹²H. Takesue, S. D. Dyer, M. J. Stevens, V. Verma, R. P. Mirin, and S. W. Nam, *Optica* **2**, 832 (2015).
- ¹³F. Najafi, J. Mower, N. C. Harris, F. Bellei, A. Dane, C. Lee, X. Hu, P. Kharel, F. Marsili, S. Assefa *et al.*, *Nat. Commun.* **6**, 5873 (2015).
- ¹⁴J. Jin, E. Saglamyurek, M. I. G. Puigibert, V. Verma, F. Marsili, S. W. Nam, D. Oblak, and W. Tittel, *Phys. Rev. Lett.* **115**, 140501 (2015).
- ¹⁵M. M. Weston, H. M. Chrzanowski, S. Wollmann, A. Boston, J. Ho, L. K. Shalm, V. B. Verma, M. S. Allman, S. W. Nam, R. B. Patel *et al.*, *Opt. Express* **24**, 10869 (2016).
- ¹⁶E. Saglamyurek, M. Grima Puigibert, Q. Zhou, L. Giner, F. Marsili, V. B. Verma, S. Woo Nam, L. Oesterling, D. Nippa, D. Oblak *et al.*, *Nat. Commun.* **7**, 11202 (2016).
- ¹⁷D. V. Reddy, R. R. Nerem, S. W. Nam, R. P. Mirin, and V. B. Verma, *Optica* **7**, 1649 (2020).
- ¹⁸P. Hu, H. Li, L. You, H. Wang, Y. Xiao, J. Huang, X. Yang, W. Zhang, Z. Wang, and X. Xie, *Opt. Express* **28**, 36884 (2020).

- ¹⁹J. Chang, J. W. N. Los, J. O. Tenorio-Pearl, N. Noordzij, R. Gourgues, A. Guardiani, J. R. Zichi, S. F. Pereira, H. P. Urbach, V. Zwiller *et al.*, *APL Photonics* **6**, 036114 (2021).
- ²⁰B. Korzh, Q.-Y. Zhao, J. P. Allmaras, S. Frasca, T. M. Autry, E. A. Bersin, A. D. Beyer, R. M. Briggs, B. Bumble, M. Colangelo *et al.*, *Nat. Photonics* **14**, 250–255 (2020).
- ²¹H. Shibata, K. Fukao, N. Kirigane, S. Karimoto, and H. Yamamoto, *IEEE Trans. Appl. Supercond.* **27**, 2200504 (2017).
- ²²V. Anant, A. J. Kerman, E. A. Dauler, J. K. W. Yang, K. M. Rosfjord, and K. K. Berggren, *Opt. Express* **16**, 10750 (2008).
- ²³L. Redaelli, G. Bulgarini, S. Dobrovolskiy, S. N. Dorenbos, V. Zwiller, E. Monroy, and J. M. Gérard, *Supercond. Sci. Technol.* **29**, 065016 (2016).
- ²⁴F. Zheng, R. Xu, G. Zhu, B. Jin, L. Kang, W. Xu, J. Chen, and P. Wu, *Sci. Rep.* **6**, 22710 (2016).
- ²⁵L. Redaelli, V. Zwiller, E. Monroy, and J. M. Gérard, *Supercond. Sci. Technol.* **30**, 035005 (2017).
- ²⁶D. V. Reddy, R. R. Nerem, A. E. Lita, S. W. Nam, R. P. Mirin, and V. B. Verma, *Conference on Lasers and Electro-Optics* (Optica, 2019), p. FF1A.3.
- ²⁷F. Ghafari, N. Tischler, J. Thompson, M. Gu, L. K. Shalm, V. B. Verma, S. W. Nam, R. B. Patel, H. M. Wiseman, and G. J. Pryde, *Phys. Rev. X* **9**, 041013 (2019).
- ²⁸L. K. Shalm, Y. Zhang, J. C. Bienfang, C. Schlager, M. J. Stevens, M. D. Mazurek, C. Abellán, W. Amaya, M. W. Mitchell, M. A. Alhejji *et al.*, *Nat. Phys.* **17**, 452–456 (2021).
- ²⁹K. Wei, W. Zhang, Y.-L. Tang, L. You, and F. Xu, *Phys. Rev. A* **100**, 022325 (2019).
- ³⁰S. N. Dorenbos, E. M. Reiger, N. Akopian, U. Perinetti, V. Zwiller, T. Zijlstra, and T. M. Klapwijk, *Appl. Phys. Lett.* **93**, 161102 (2008).
- ³¹D. Henrich, L. Rehm, S. Dorner, M. Hofherr, K. Il'in, A. Semenov, and M. Siegel, *IEEE Trans. Appl. Supercond.* **23**, 2200405 (2013).
- ³²J. Huang, W. J. Zhang, L. X. You, X. Y. Liu, Q. Guo, Y. Wang, L. Zhang, X. Y. Yang, H. Li, Z. Wang *et al.*, *Supercond. Sci. Technol.* **30**, 074004 (2017).
- ³³V. B. Verma, F. Marsili, S. Harrington, A. E. Lita, R. P. Mirin, and S. W. Nam, *Appl. Phys. Lett.* **101**, 251114 (2012).
- ³⁴C. Gu, Y. Cheng, X. Zhu, and X. Hu, *Advanced Photonics 2015* (Optica, 2015), p. JM3A.10.
- ³⁵X. Chi, K. Zou, C. Gu, J. Zichi, Y. Cheng, N. Hu, X. Lan, S. Chen, Z. Lin, V. Zwiller *et al.*, *Opt. Lett.* **43**, 5017 (2018).
- ³⁶Y. Meng, K. Zou, N. Hu, X. Lan, L. Xu, J. Zichi, S. Steinhauer, V. Zwiller, and X. Hu, *Opt. Lett.* **45**, 471 (2020).
- ³⁷Y. Meng, K. Zou, N. Hu, L. Xu, X. Lan, S. Steinhauer, S. Gyger, V. Zwiller, and X. Hu, “Fractal superconducting nanowires detect infrared single photons with 84% system detection efficiency, 1.02 polarization sensitivity, and 20.8 ps timing resolution,” *ACS Photonics* (published online).
- ³⁸J. R. Clem and K. K. Berggren, *Phys. Rev. B* **84**, 174510 (2011).
- ³⁹R. Xu, F. Zheng, D. Qin, X. Yan, G. Zhu, L. Kang, L. Zhang, X. Jia, X. Tu, B. Jin *et al.*, *J. Lightwave Technol.* **35**, 4707–4713 (2017).
- ⁴⁰A. Mukhtarova, L. Redaelli, D. Hazra, H. Machhadani, S. Lequien, M. Hofheinz, J.-L. Thomassin, F. Gustavo, J. Zichi, V. Zwiller *et al.*, *Opt. Express* **26**, 17697 (2018).
- ⁴¹R. Xu, Y. Li, F. Zheng, G. Zhu, L. Kang, L. Zhang, X. Jia, X. Tu, Q. Zhao, B. Jin *et al.*, *Opt. Express* **26**, 3947 (2018).
- ⁴²D. Li and R. Jiao, *Photonics Res.* **7**, 847 (2019).
- ⁴³A. N. McCaughan, A. N. Tait, S. M. Buckley, D. M. Oh, J. T. Chiles, J. M. Shainline, and S. W. Nam, *J. Vac. Sci. Technol., B* **39**, 062601 (2021).
- ⁴⁴C. Yang, M. Si, X. Zhang, A. Yu, J. Huang, Y. Pan, H. Li, L. Li, Z. Wang, S. Zhang *et al.*, *Opt. Express* **29**, 21400 (2021).
- ⁴⁵Y. P. Korneeva, N. Manova, I. Florya, M. Y. Mikhailov, O. Dobrovolskiy, A. Korneev, and D. Y. Vodolazov, *Phys. Rev. Appl.* **13**, 024011 (2020).
- ⁴⁶J. Chiles, S. M. Buckley, A. Lita, V. B. Verma, J. Allmaras, B. Korzh, M. D. Shaw, J. M. Shainline, R. P. Mirin, and S. W. Nam, *Appl. Phys. Lett.* **116**, 242602 (2020).
- ⁴⁷D. Vodolazov, N. Manova, Y. Korneeva, and A. Korneev, *Phys. Rev. Appl.* **14**, 044041 (2020).
- ⁴⁸I. Charaev, Y. Morimoto, A. Dane, A. Agarwal, M. Colangelo, and K. K. Berggren, *Appl. Phys. Lett.* **116**, 242603 (2020).
- ⁴⁹A. E. Lita, V. B. Verma, J. Chiles, R. P. Mirin, and S. W. Nam, *Supercond. Sci. Technol.* **34**, 054001 (2021).
- ⁵⁰S. Steinhauer, S. Gyger, and V. Zwiller, *Appl. Phys. Lett.* **118**, 100501 (2021).
- ⁵¹X. Zhang, I. Charaev, H. Liu, T. X. Zhou, D. Zhu, K. K. Berggren, and A. A. Schilling, *Supercond. Sci. Technol.* **34**, 095003 (2021).
- ⁵²G.-Z. Xu, W.-J. Zhang, L.-X. You, J.-M. Xiong, X.-Q. Sun, H. Huang, X. Ou, Y.-M. Pan, C.-L. Lv, H. Li *et al.*, *Photonics Res.* **9**, 958 (2021).
- ⁵³J. K. W. Yang, A. J. Kerman, E. A. Dauler, B. Cord, V. Anant, R. J. Molnar, and K. K. Berggren, *IEEE Trans. Appl. Supercond.* **19**, 318–322 (2009).
- ⁵⁴R. Baghdadi, E. Schmidt, S. Jahani, I. Charaev, M. G. W. Müller, M. Colangelo, D. Zhu, K. Ilin, A. D. Semenov, Z. Jacob *et al.*, *Supercond. Sci. Technol.* **34**, 035010 (2021).
- ⁵⁵J.-M. Xiong, W.-J. Zhang, G.-Z. Xu, L.-X. You, X.-Y. Zhang, L. Zhang, C.-J. Zhang, D.-H. Fan, Y.-Z. Wang, H. Li, and Z. Wang, *Supercond. Sci. Technol.* **35**, 055015 (2022).
- ⁵⁶M. Jönsson, R. Vedin, S. Gyger, J. A. Sutton, S. Steinhauer, V. Zwiller, M. Wallin, and J. Lidmar, *arXiv:2112.05443* (2021).
- ⁵⁷M. G. Moharam and T. K. Gaylord, *J. Opt. Soc. Am.* **71**, 811 (1981).
- ⁵⁸H. Li, S. Chen, L. You, W. Meng, Z. Wu, Z. Zhang, K. Tang, L. Zhang, W. Zhang, X. Yang *et al.*, *Opt. Express* **24**, 3535 (2016).
- ⁵⁹A. J. Miller, A. E. Lita, B. Calkins, I. Vayshenker, S. M. Gruber, and S. W. Nam, *Opt. Express* **19**, 9102 (2011).
- ⁶⁰S. Liu, X.-R. Yao, X.-F. Liu, D.-Z. Xu, X.-D. Wang, B. Liu, C. Wang, G.-J. Zhai, and Q. Zhao, *Opt. Express* **27**, 22138 (2019).
- ⁶¹B. Li, G. Deng, R. Zhang, Z. Ou, H. Zhou, Y. Ling, Y. Wang, Y. Wang, K. Qiu, H. Song, and Q. Zhou, *J. Lightwave Technol.* **37**, 5899 (2019).
- ⁶²P. B. Coates, *J. Phys. E: Sci. Instrum.* **1**, 878–879 (1968).
- ⁶³J. G. Walker, *Opt. Commun.* **201**, 271–277 (2002).